Desalination and Water Treatment
www.deswater.com

doi: 10.1080/19443994.2016.1163736

57 (2016) 27199–27212
December

Taylor & Francis
Taylor & Francis Group

Experimental and modeling study on adsorption of cationic methylene blue dye onto mesoporous biochars prepared from agrowaste

Ali Akbar Babaei[a,b], Seyed Nadali Alavi[c,d], Mitra Akbarifar[e], Kamal Ahmadi[b], Amirhosein Ramazanpour Esfahani[f], Babak Kakavandi[a,b,e,*]

[a]*Environmental Technologies Research Center, Ahvaz Jundishapur University of Medical Sciences, Ahvaz, Iran, Tel. +98 611 3738269; emails: ababaei52@gmail.com (A.A. Babaei), kakavandibvch@ajums.ac.ir (B. Kakavandi)*
[b]*Department of Environmental Health Engineering, School of Public Health, Ahvaz Jundishapur University of Medical Sciences, Ahvaz, Iran, Tel. +98 611 3738269; email: ahmadikamal56@yahoo.com (K. Ahmadi)*
[c]*Environmental and Occupational Hazards Control Research Center, Shahid Beheshti University of Medical Sciences, Tehran, Iran*
[d]*Department of Environmental Health Engineering, School of Public Health, Shahid Beheshti University of Medical Sciences, Tehran, Iran, Tel. +98 2122432040; email: alavi@sbmu.ac.ir*
[e]*Student Research Committee, Ahvaz Jundishapur University of Medical Sciences, Ahvaz, Iran, Tel. +98 611 3738269; email: mitra.akbarifar@yahoo.com (M. Akbarifar)*
[f]*Faculty of Agriculture, Department of Soil Science, Shahid Chamran University of Ahvaz, Iran, Tel. +98 613 3364054; email: ramazanpour67@gmail.com*

Received 27 February 2015; Accepted 3 March 2016

ABSTRACT

Oak wood, an agrowaste, was activated to prepare biochar and used as an effective biosorbent to remove methylene blue (MB) dye from aqueous solution. The properties of the adsorbent were also characterized using scanning electron microscope, Brunauer–Emmett–Teller, and Fourier Transform Infrared techniques. The adsorption process was studied in a batch system by investigating the effects of different experimental variables such as pH of solution, contact time, adsorbent dosage, initial dye concentration, temperature, and adsorbent particle size. The equilibrium time was obtained as 120 min. The adsorption process was fully described by the Liu equilibrium and pseudo-second-order kinetic models. The maximum adsorption capacity obtained was 97.55 mg/g based on the Langmuir isotherm at 50°C. The activation energy was found to be 24.2 kJ/mol, which indicated the feasibility of the adsorption process. The values of thermodynamic parameters (ΔG°, ΔS°, and ΔH°) showed that the adsorption of MB dye onto the biochar surfaces was spontaneous, feasible, and endothermic. The biochar was also found to enjoy a good performance for the removal of MB in real wastewater samples under optimum experimental conditions. So, it can be concluded that biochar can be utilized as a cost-effective, environmental-friendly, and promising adsorbent for the removal of dyes from colored wastewaters.

Keywords: Methylene blue; Equilibrium; Adsorption; Low cost adsorbent; Biochar

*Corresponding author.

1. Introduction

Wastewater containing dyes derived from industry discharges is recently increasing in volume, due to the fact that they are widely used for various purposes (e.g. in chemical laboratories for analytical purposes and in many biological and biomedical laboratories as stains) [1]. Moreover, in textile, paper and photographic manufactures, dyes are used for painting products, which has caused serious health and environmental risks around the world [1,2]. Dyes are very toxic substances and contain carcinogenic compounds which can trigger permanent health damages to the eyes and the skin of both humans and animals. They also reduce light penetration in aquatic environments, bringing about negative effects on photosynthesis. Therefore, regarding the aforementioned negative effects, structure and stability of these compounds, their complete removal from potable water resources and wastewaters is a critical necessity [2,3].

A wide spectrum of treatment processes including adsorption, coagulation and flocculation, biodegradation, chemical and photochemical decomposition, membrane separation [1,2], and advanced oxidation and extraction have been applied to study the removal of dyes from aqueous solution [4]. However, most of these techniques are expensive and suffer from the problem of sludge disposal [1]. Among these methods, the adsorption process, which is widely employed, has proved to be a suitable option for the treatment of dyed wastewater since using this process is simple, requires slight maintenance, and produces the least sludge [5–8]. Furthermore, the preparation and also access to the adsorbents with low cost are apparently possible. They have also shown high performance in being used for the quick control of pollutants [1,9].

In the adsorption process, activated carbon (AC) prepared from different raw materials represents the most effective adsorbent. AC, with respect to unique characteristics such as high surface areas, porous structure, and high adsorption capacity, has shown a high potential in dye substances removal. However, their expensive restoration and production caused limitations against their application. Most scientists tried to find novel and cheap adsorbents, so lots of research have been performed to develop the use of low-cost adsorbents [1,10]. In order to remove organic and inorganic contaminants, researchers have used various natural adsorbents such as charcoal, waste oak [11], Olive seeds [12], rice husk [10,13] and rice straw [13], coconut (*Cocos nucifera*) bunch waste [14], solid wastes and sewage sludge [15,16], crop straw [17,18], camphor wood [4], pine wood [19], sunflower seed [20], and sugar beet tailings [21].

In recent years, adsorption of contaminants by biochar has increasingly received a lot of attentions as an environmentally friendly alternative and a mitigation strategy to climate change. Biochar, as a carbon-rich, stable, and porous material, is generated by the thermal decomposition of biomass under oxygen-limited conditions (pyrolysis) and heated at a relatively low temperature (<700˚C) [22]. Biochar has several useful intrinsic features such as high porosity, high oxygen-containing functional groups, high alkalinity, high adsorption capacity, high specific surface area [17,23], and hydrophobic characteristics [24]. Various types of raw materials like woodchips, animal manures, crop residues, and solid wastes can be applied as a biochar source because they increase the recycling of agricultural and forestry waste, and this is one of the considerable advantages of biochars [22]. Biochars have proved the ability of being resistant to chemical and biological degradation [15].

The aim of this study was to investigate the performance of oak wood biochar for the removal of methylene blue (MB) dye from aqueous solution. Herein, we used alkaline treated oak wood biochar (labeled as ATOB) as an inexpensive and locally available material for the preparation of the adsorbent. In this study, parameters affecting the performance of adsorption, including pH of solution, the contact time, the amounts of adsorbent, the temperature, and the initial dye concentration were investigated. Finally, the equilibrium isotherm and kinetic models were studied to evaluate and fit the experimental data.

2. Materials and methods

All chemicals were of analytical laboratory grade, purchased from Merck. Co, and used without further purification. MB (empirical formula $C_{16}H_{18}ClN_3S{\cdot}3H_2O$; molecular weight 373.9 g/mol) was used as the adsorbate. The chemical structure of MB, as shown in Fig. 1 has a maximum visible absorbance at the wavelength of 661 nm. The MB stock solution (1,000 mg/L) was prepared by dissolving MB in distilled water, and subsequently diluted to the required concentrations.

2.1. Preparation of ATOB

The oak wood pieces that fell under the trees were used as raw materials. They were collected from indigenous areas located in the north of Khuzestan Province, Iran. Oak biochar was prepared through slow pyrolysis inside a furnace in an oxygen-free environment at temperatures of 450–600˚C. It was then

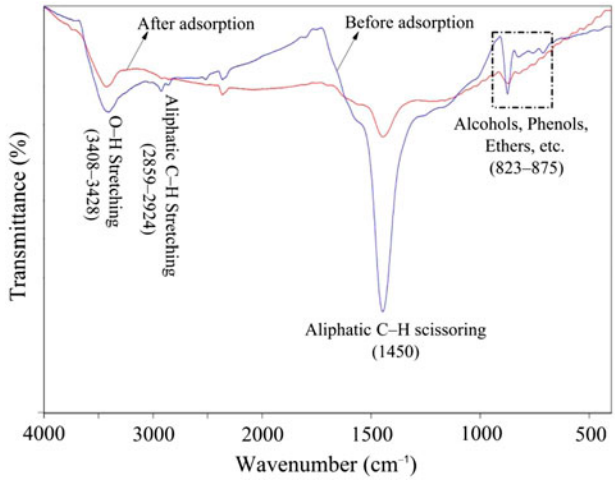

Fig. 1. FTIR spectra of ATOB before and after MB adsorption.

immersed in 1 M sodium hydroxide solution (NaOH 1 M) for 1 h. NaOH solution was used to increase the number of active surfaces and to prevent the elution of tannin compounds that would otherwise stain the treated water and increase the COD of the solution. The sample was then washed with distilled water repeatedly to remove NaOH. After drying at 105°C for 48 h, the sample was crushed and passed through a range of sieves with different sizes. Only particles with mesh sizes between 250 and 100 μm were used in accordance with the ASTM Method [25]. After sieving, the sample was dried in an oven at 80–85°C for 2 h and then stored in plastic bags until use.

2.2. Features of ATOB

The physical characteristics of ATOB, namely the bulk density, the particle size, and the specific surface area, were investigated. The bulk density and particle size of adsorbent samples were determined using Gay–Lussac pycnometer and sieve analysis, respectively. The specific surface area of the ATOB, measured by nitrogen adsorption/desorption apparatus (Quantachrome, 2000, NOVA) and Brunauer–Emmett–Teller (BET) model, was found to be 245.7 m^2/g. The chemical properties of the ATOB were characterized by moisture, water soluble and insoluble compounds, volatile fraction, ash, and elemental analysis. The moisture and ash content were measured using a digital microprocessor-based moisture analyzer (Mettler LP16) and ASTM D2866–11, respectively. CHNOS-Rapid Elemental Analytical Instrument (Elementer, Germany) was used for the elemental analysis of the adsorbent. The pH of point of zero charge (pH_{pzc}) of the ATOB was determined accordingly with the procedure reported in the literature [26]. Physical and chemical properties of the ATOB are presented in Table 1.

Table 1
Physical and chemical characteristics of ATOB

Characteristics	Values
Physical	
Bulk density (kg/m^3)	395
Particle size (μm)	100–250
Specific surface area (m^2/g)	245.7
Chemical	
pH_{PZC}	8.5
Moisture	2.1 (±0.7)
Water-soluble compounds	2 (±0.8)
Insoluble compounds	95.9 (±0.4)
Volatile fraction	13.3 (±0.8)
Fixed carbon	77.2 (±0.5)
Ash content	5.4 (±0.8)
Elemental analysis (%)	
C	85.5
H	2.4
N	0.5
O (by difference)	11.6
S	Not detected

The size and surface morphologies of the adsorbent were analyzed using a scanning electron microscope (SEM) (Philips XL-20). BRUKER's Vertex 70 infrared spectrometer was also used for the Fourier transform infrared (FTIR) spectroscopy to find functional groups onto the surfaces of the applied adsorbent.

2.3. Batch adsorption procedure

The effects of input variables such as pH of solution, contact time, adsorbent dosage, initial MB concentrations, solution temperature, and particles size on the adsorption efficiency were investigated in a batch system. The experiments regarding the adsorption of MB onto the ATOB surface were conducted in 100 mL Erlenmeyer flasks containing 50 mL of MB solution and varying adsorbent dosages. Then, the samples were shaken at a constant rate of 300 rpm to reach adsorption equilibrium conditions. Afterwards, to separate the adsorbents from MB solution, samples were centrifuged at 5,000 rpm for around 5 min. At final step, the residual concentrations of MB were measured using a UV–visible spectrophotometer (DR-5000, Hach Co.) at its maximum absorbance wavelength,

661 nm. All the experiments were conducted in triplicate and the mean values were presented as final results. The adsorption capacity (q_e) and the removal efficiency (R) of MB dye were obtained employing the following equations:

$$q_e = \frac{(C_o - C_e)V}{m} \quad (1)$$

$$R = \frac{C_o - C_e}{C_o} \times 100 \quad (2)$$

where q_e (mg/g) is the amount of adsorbed MB onto the unit amount of the adsorbent, C_o and C_e (mg/L) are the initial and equilibrium MB concentrations, respectively, V (L) is the volume of the solution, and m (g) is the adsorbent mass in dry form.

2.4. MB adsorption optimization

To optimize the variables affecting MB adsorption, the effects of pH in the range of 2–11 were investigated during 60 min at 25 ± 1°C. The pH of solution was adjusted by adding 0.1 M HCl and 0.1 M NaOH solution. The effects of contact time and the subsequent kinetics of the adsorption were studied at different initial MB concentrations (25–100 mg/L) for a period of 5 h. Afterwards, the adsorption isotherms were investigated across various ATOB concentrations (0.1–10 g/L) and solution temperatures of 5, 25, and 50°C. To calculate the values of thermodynamic parameters, the effects of solution temperature on the adsorption behavior of MB dye was studied in the range of 5–50°C. The effects of the different sizes of the ATOB particles were also performed in two different size ranges of 210–250 μm and 53–63 μm for varying dosages of adsorbent. At the end, real wastewater samples containing different initial concentrations of MB were investigated in order to verify the efficiency of biochar for the removal of dyes from textile industry effluents.

2.5. Modeling MB adsorption

2.5.1. Adsorption kinetic and isotherm models

The control mechanism of the adsorption process of MB onto the ATOB was evaluated using non-linear kinetic equations. Hence, six widely used kinetic models including pseudo-first-order, pseudo-second-order, Elovich, intraparticle diffusion, fractional power, and Avrami fractional order were applied to analyze the obtained data of adsorption experiments.

The adsorption isotherms are characterized by certain constant values. These values express the surface properties and the affinity of the adsorbent. Also, when the adsorption process reaches an equilibrium state, these values become significant in describing how the adsorbate molecules distribute between the liquid and the solid phases [27–29]. Additionally, in the present study, Langmuir, Freundlich, Liu, Redlich–Peterson (R–P) and Temkin equilibrium isotherm models were used to predict the behavior of MB adsorption and to describe the adsorption capacity of ATOB. Langmuir and Freundlich isotherm models are based on the homogeneous (single-layer) and the heterogeneous (multi-layer) adsorption of adsorbate onto the adsorbent surfaces, respectively. The Redlich–Peterson isotherm model, on the other hand, describes adsorption on both homogeneous and heterogeneous surfaces. Therefore, this model has both of the features of the equilibrium models of Langmuir and Freundlich [30]. Finally, Temkin equilibrium model is based on indirect interactions of adsorbate and adsorbent. It also suggests that the heat of the adsorption decreases linearly [31]. All the used mathematical isotherm and kinetic models are summarized in Supplementary data, Table S-1.

The favorability of MB adsorption onto the ATOB was examined using a dimensionless parameter, R_L ($R_L = 1/(1 + K_L C_o)$), derived from the Langmuir model. The type of isotherm is determined by R_L values according to the following categories:

Unfavorable ($R_L > 1$), favorable ($0 < R_L > 1$), irreversible ($R_L = 0$), and linear adsorption ($R_L = 1$) [6].

2.5.3. Fitness of kinetic and isotherm models

To select the most suitable kinetic and isotherm models, it is necessary to evaluate their validity. Hence, in this study, apart from the correlation coefficient (R^2), the adjusted determination factor (R^2_{adj}, the sum of squared error (SSE), and the root mean square error (RMSE) were also used as criteria for the goodness of fit between the experimental and predicted data. The calculated R^2, R^2_{adj}, SSE, and RMSE values are represented in Supplementary data, Table S-2. The smaller RMSE and SSE values as well as the R^2_{adj} and R^2 values close to one suggest the best and the most valid model.

2.6. Preparation of simulated dye house effluent

To imitate the effluents containing reactive dyes produced by typical textile industries, a simulated dye house effluent containing five typical dyes commonly

Table 2
The characteristics of the simulated dye house effluent

	Concentration (mg/L)
Dyes	
Cibacron brilliant yellow 3G-P (λ_{max} 402 nm)	10–100
Reactive red M-2BE (λ_{max} 505 nm)	5.0
Reactive black 5 (λ_{max} 598 nm)	5.0
Reactive orange 16 (λ_{max} 489 nm)	5.0
Methylene blue (λ_{max} 661 nm)	5.0
Auxiliary chemicals	
Na_2SO_4	100
NaCl	100
Na_2CO_3	150
CH_3COONa	300
CH_3COOH	100
pHa	7.0

used as fabric colorants together with auxiliary chemicals was prepared at pH 7.0. Typically, between 10 and 60% of synthetic dyes and almost the entire dye bath auxiliaries remain in the spent dye bath and its composition is diluted 5–30 folds during the next regular washing and rinsing steps [32,33]. The characteristics of the simulated dye house effluent are summarized in Table 2.

3. Results and discussion

3.1. Adsorbent properties

The adsorbent was characterized by FTIR in a nearby IR region (wave number: 400–4,000 cm^{-1}). The FTIR spectra (Fig. 1) displayed some absorption peaks belonging to various functional groups or different vibration modes. The wave number of 3,400–3,450 cm^{-1} indicates the hydroxyl (–OH) stretching, while the bands at about 2,900 cm^{-1} are attributed to the aliphatic C–H stretching. The band at around 1,450 cm^{-1}, which is a peak very strong, can be probably from some vibration of inorganic ingredients. The band at 875 cm^{-1} was found relevant to the presence of primary, secondary, and tertiary alcohols, phenols, ethers, and esters showing C–O stretching and O–H deformation vibrations [34]. These functional groups may form surface complexes with MB dye and thus can increase the specific adsorption of MB by biochar. A comparison between the FTIR spectra of the ATOB before and after the adsorption of MB dye illustrates that MB adsorption brings about changes in absorption frequencies at 875, 2,900, and 3,400 cm^{-1}, which are presented in the surface of the adsorbent. It seems that the mentioned functional groups influence the MB adsorption on the ATOB.

The SEM images of the ATOB are presented in Fig. 2. The SEM images show that the adsorbent consists of irregular plates and has a porous structure, which favored effective adsorption sites. The BET surface area of the ATOB was 245.7 $m^2 g^{-1}$, indicating the porous structure of the adsorbent. The surface area of the ATOB in the present study was much higher than that of the oak bark char and the magnetic oak wood biochar reported by Mohan et al. and Mohan et al., respectively [35,36].

3.2. Effect of pH

The pH of solution, due primarily to its significant effects on surface functional groups of adsorbents and adsorbate features is one of the most influential

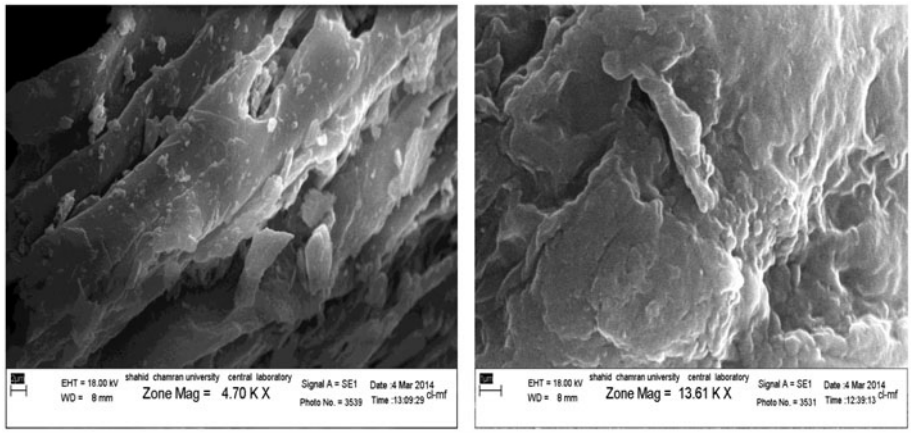

Fig. 2. SEM micrograph of ATOB.

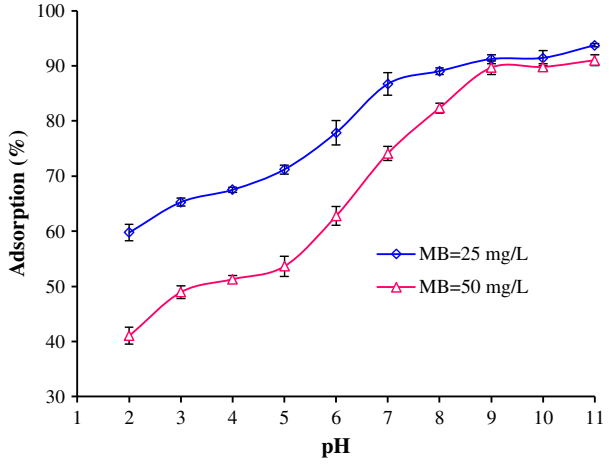

Fig. 3. Effect of pH on the MB dye adsorption by ATOB (contact time: 60 min, adsorbent dose: 5 g/L, T = 25 ± 1˚C).

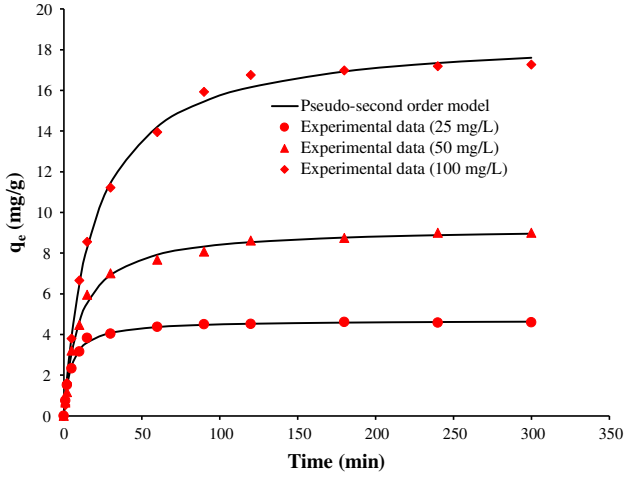

Fig. 4. Non-linear pseudo-second-order kinetic model of MB adsorption on biochar (pH 7.0 ± 0.1, adsorbent dose: 5 g/L, T = 25 ± 1˚C).

parameters in the adsorption process. The results of the effects of pH variations on the percentage of MB adsorption by the ATOB are presented in Fig. 3. As can be seen, MB adsorption percentages increased with the increase in pH from 2 to 9 for both 25–50 mg/L dye concentrations. The removal efficiency by the ATOB showed an increase from 40–60 to 90% with an increase in the pH values from 2.0 to 9.0. The removal efficiency then remained almost constant at higher pH values. The pH value of the ATOB at the point of zero charge (pH_{PZC}) was found to be 8.5 as shown in Table 1. This means that at pH > pH_{pzc}, the biochar surface becomes negatively charged, due to the presence of hydroxide ions (OH^-) and, consequently, the MB cations are easily adsorbed onto this surface by electrostatic attraction forces. Thus pH values greater than 8.5 will be favorable for MB adsorption on the ATOB.

On the other hand, at pH < pH_{pzc}, the surface of the adsorbent is positive leading to an electrostatic repulsion between MB cations and the biochar, which results in a decrease in the adsorption percentage. Moreover, under acidic pH conditions, the H^+ ions exist at high concentrations, which compete with dye cations for active sites onto the ATOB surfaces. Hence, based on the fact that most sewage and water bodies have the pH ranges at about neutral (6.0–8.0), pH 7.0 ± 0.1 was selected as the optimum value in all the accompanying experiments.

3.3. MB adsorption kinetic

In this investigation, the effects of contact time and adsorption kinetic were studied at a period of 0–300 min, with the optimum pH of 7.0 ± 0.1 and adsorbent dosage of 5 g/L at 25 ± 1˚C for different MB concentrations. As shown in Fig. 4, the adsorption capacity of MB is increased rapidly during the first 60 min and then reached the equilibrium point after 120 min. The rapid increase in the adsorption capacity in the initial stages may be derived from the existence of enormous vacant active sites onto the adsorbent surfaces [7]. However, increasing the contact time resulted in a decrease in the availability of MB molecules to active sites on the ATOB surfaces and reduced the adsorption efficiency. Other researchers have observed the same phenomenon in the investigation of MB adsorption on different adsorbents [3,27,37,38]. It was concluded that 120 min were sufficient for the adsorption to reach equilibrium.

Results from the study of kinetic models showed that the adsorption kinetics of MB can be described by the pseudo-second-order model. The values of the kinetic model parameters of the MB adsorption on the ATOB are listed in Table 3. The validity of the studied models is verified by the criteria of R^2_{adj}, SSE, and RMSE. The high R^2_{adj} and low SSE and RMSE of the pseudo-second-order model, compared with others, indicate that the pseudo-second-order model provides a better fitting to the experimental data. The confirmation of this model suggests that the concentrations of both adsorbent and adsorbate are associated with the rate-determining step of the adsorption process [5]. In addition, Table 3 indicates that the calculated amount of adsorption capacity ($q_{e,cal}$) from pseudo-second-order model matches quite well with the experimental data ($q_{e,exp}$). This finding is also confirmed by

Table 3
Kinetic parameters of MB adsorption onto ATOB at initial different concentrations

Adsorption kinetic models	Parameters	Initial MB concentration		
		25 mg/L	50 mg/L	100 mg/L
Pseudo-first-order				
	q_e (mg/g)	4.45	8.5	16.7
	K_f (min^{-1})	0.1436	0.0759	0.04243
	RMSE	0.2047	0.4244	0.6946
	SSE	0.461	1.981	5.307
	R^2_{adj}	0.984	0.984	0.99
Pseudo-second-order				
	k_S (g mg/min)	0.0461	0.0107	0.0028
	q_e (mg/g)	4.708	9.253	18.73
	RMSE	0.093	0.22	0.327
	SSE	0.096	0.533	1.178
	R^2_{adj}	0.997	0.996	0.998
P–F				
	a	1.868	2.403	3.341
	b	0.1789	0.2525	0.3122
	RMSE	0.5732	1.068	1.936
	SSE	3.614	12.54	41.24
	R^2_{adj}	0.87	0.9	0.92
Avrami fractional order				
	k_{AV} (min^{-1})	0.1308	0.0653	0.0366
	q_e (mg/g)	4.53	8.69	17.22
	n_{AV}	0.7347	0.7731	0.7915
	RMSE	0.1175	0.3624	0.4016
	SSE	0.138	1.313	1.613
	R^2_{adj}	0.995	0.989	0.997
Elovich				
	α (mg g/min)	4.844	2.263	1.933
	β (g/mg)	1.505	0.6155	0.2657
	RMSE	0.4157	0.6442	1.043
	SSE	1.901	4.565	11.97
	R^2_{adj}	0.934	0.964	0.977
Intraparticle diffusion				
	k_{id} (mol/g $min^{1/2}$)	0.2256	0.515	1.088
	C	1.705	2.031	2.37
	RMSE	0.9865	1.626	2.691
	SSE	10.71	29.09	79.67
	R^2_{adj}	0.63	0.77	0.85

the curves presented in Fig. 4. This is in good agreement with the previous studies for MB adsorption on carbon nanotubes [27], graphite powder [39], and coir pith carbon [40].

Other models (i.e. pseudo-first-order, P–F, Avrami, Elovich, and intraparticle diffusion) present the lower R^2_{adj} and higher SSE and RMSE values, compared to pseudo-second-order model, indicating that these models could not fit properly the experimental kinetic data. In this study, the intraparticle diffusion model was not only employed to understand the mechanism of adsorption process but also to predict the rate-controlling step. However, based on the obtained results, it was found that this model plays less significant role in the adsorption process. As observed in Table 3, the values of $C_i > 0$ reveal that intraparticle dif-

fusion is not the only controlling step for MB adsorption on the ATOB; and also, the process is controlled to some degrees by boundary layer diffusion [30].

3.4. MB adsorption isotherm

Equilibrium study is very important for determining the adsorption capacity as well as designing and operating the adsorption process. The adsorption isotherm studies were carried out with the initial MB concentration range of 25–100 mg/L, the pH of 7.0 ± 0.1, and the adsorbent dosage of 0.1–10 g/L for 120 min contact time at various temperatures. Referring to Table 4, we can see that the values of q_e have increased from 39.5 to 90.4 mg/g by increasing the initial MB concentration from 25 to 100 mg/L. The increase in C_o enhanced dramatically the interaction between the adsorbent and MB. This phenomenon would be attributed to the increased force of concentration gradient.

As can be observed in Table 4, the sorption capacity for the initial MB concentration of 50 mg/L increased from 32.84 to 97.55 mg/g with the increasing temperatures from 5 to 50˚C. The effect of temperature is fairly common and increases the diffusion of the dye cations. Furthermore, an increase in temperature may cause the swelling effects within the internal structure of the adsorbent, enabling more penetration of MB molecules into the ATOB pores. The increase in the adsorption yield and adsorption capacity at high temperatures indicated that the adsorption of MB dye by the ATOB may involve both physical and chemical sorption. This can be due to an increase in bond rupture, and consequently, an increase in active sites at high temperatures [41].

Table 4 shows the obtained values of equilibrium isotherm parameters of the MB adsorption onto the ATOB surfaces. It is clear that Liu model showed the lowest RMSE and SSE values. It is also noticeable that the values of R^2_{adj} in Liu isotherm model are higher than these values in other models. In addition, the best fit is obtained through combining the Liu model by employing a nonlinear method (Fig. 5). As it is observed in Table 4, the values of R_L and $1/n$ are both less than one, which suggests MB cations are favorably adsorbed on the ATOB surface [3]. As can be seen from Table 4, the maximum adsorption capacities based on the Langmuir model enhanced with increasing solution temperature, which is an indicator of the endothermic nature of the adsorption of MB onto the ATOB surfaces.

Despite the fact that the Redlich–Peterson (R–P) model was the best isotherm model for MB adsorption by the ATOB adsorbent based on R^2_{adj}, RMSE and SSE parameters, this isotherm model is invalid since g is more than one. The Temkin isotherm assumes that the heat adsorption of molecules in the layer decreases linearly with coverage due to adsorbate and adsorbent interactions. This model also assumes that a multilayer adsorption on a surface occurred, the binding energy of the sites is unequivalent, and the adsorbent interacts with the adsorbed molecules. However, the values of the R^2_{adj} of the Temkin was low for all studied temperatures. This means that the Temkin model is not suitable to describe the adsorption equilibrium process.

3.5. Comparison of biochar maximum adsorption capacity with literature data

The maximum adsorption capacity, q_m, of the ATOB was compared with the MB adsorption capacities for other adsorbents (Table 5). The maximum amount of MB uptake per unit mass of the ATOB was 90.46 mg/g based on the Liu equilibrium model. It is noticeable from Table 5 that the ATOB has a good maximum adsorption capacity in comparison with the other applied adsorbents.

3.6. MB adsorption thermodynamic

In this study, thermodynamic parameters of MB adsorption on the ATOB were determined at various temperatures of 5–50˚C under optimum experimental conditions. Arrhenius activation energy (E_a), entropy change (ΔS°), enthalpy change (ΔH°), and Gibbs free energy change (ΔG°) are the thermodynamic parameters of the adsorption process. The value of E_a was calculated using the following equation:

$$\ln k_S = \ln k_o - \frac{E_a}{RT} \tag{3}$$

where k_o is the Arrhenius factor, R is the gas constant (8.3145 J/mol K), and k_S is the pseudo-second rate constant (min^{-1}) at temperature T. A linear plot of ln k_S vs. $1/T$ for the adsorption of MB onto the ATOB surfaces was plotted to determine the E_a value from the slope using the Arrhenius equation (Fig. 6). The E_a was found to be 24.2 kJ/mol at pH 7.0 ± 0.1 with a $R^2 > 0.997$. The physisorption process has activation energies in the range of 5–40 kJ/mol, hence it can be concluded that the adsorption of MB onto the ATOB was a physisorption process [56]. The positive values of E_a also indicate the feasibility of the adsorption process.

Table 4
Values of the equilibrium parameters of MB adsorption onto ATOB at different temperatures

Adsorption isotherm models	Parameters	T (°C)		
		5	25	50
Langmuir				
	q_m (mg/g)	32.84	55.7	97.55
	K_L (L/mg)	0.043	0.084	0.08
	R_L	0.317	0.192	0.2
	R^2_{adj}	0.9881	0.91	0.887
	RMSE	0.750	5.67	11.26
	SSE	2.813	193	634.2
Freundlich				
	K_F (L/g)	2.753	5.035	7.803
	n	1.83	1.613	1.498
	R^2_{adj}	0.9553	0.96	0.9432
	RMSE	1.456	3.744	8.01
	SSE	10.6	70.07	320.8
Redlich–Peterson				
	K_{RP} (L/g)	1.133	2.126	3.608
	a_{RP} (L/mg)	0.0061	0.0005	0.0001
	g (–)	1.423	1.96	2.952
	R^2_{adj}	0.993	0.984	0.994
	RMSE	0.5776	2.348	2.601
	SSE	1.335	22.06	27.06
Liu				
	K_g (L/mg)	0.0433	0.065	0.09
	n	0.95	1.669	1.866
	q_m (mg/g)	32.53	57.6	90.46
	R^2_{adj}	0.997	0.985	0.991
	RMSE	0.3553	2.324	3.142
	SSE	0.505	21.61	39.48
Temkin				
	A_T (L/g)	0.3816	1.007	1.034
	B	7.622	12.03	20.3
	R^2_{adj}	0.9959	0.82	0.7801
	RMSE	0.4419	7.903	15.76
	SSE	0.9764	312.3	1,242

The values of ΔS° and ΔH° were obtained from the intercept and slope of vant Hoff plots of ln K vs. $1/T$ according to the following equation:

$$\ln(K) = \frac{\Delta S^\circ}{R} - \frac{\Delta H^\circ}{RT} \quad (4)$$

where K represents the equilibrium adsorption constants of the Langmuir isotherm fits. The calculated values of the thermodynamic parameters are presented in Table 6. It is observed that ΔH° has a positive value, indicating the adsorption process has been endothermic in nature. The values of $\Delta H^\circ < 40$ kJ/mol suggest that MB adsorption on the ATOB has a physisorption mechanism [57,58]. The positive value of ΔS° confirms increasing randomness at the solid/solution interface with some structural changes in the adsorbate and adsorbent during the adsorption process. This result is in good agreement with other studies on the adsorption of reactive dyes onto peanut hull [59].

The values of ΔG° were also calculated from the Gibbs free energy equation:

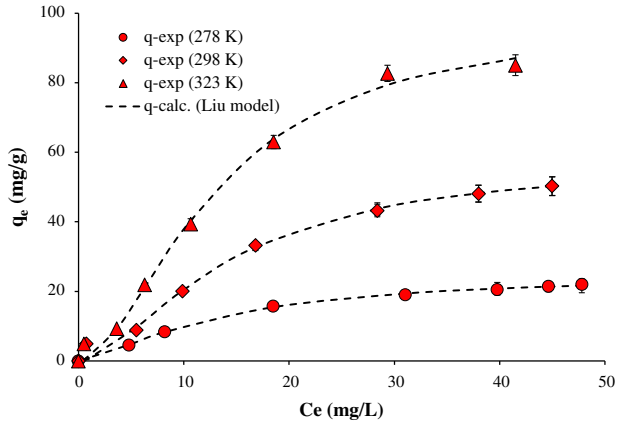

Fig. 5. Non-linear plots of Liu isotherm model of MB adsorption on ATOB at different temperatures (pH 7.0 ± 0.1, contact time: 120 min, MB: 50 mg/L and adsorbent dose: 0.1–10 g/L).

$$\Delta G^{\circ} = -RT\ln(K) \quad (5)$$

From Table 6, it can be seen that ΔG° values are negative at all the three studied temperatures. The negative ΔG° values reflect the spontaneous nature of the process of adsorption. Table 5 also shows that raising the temperature leads to greater negative ΔG° values, implicating that the adsorption process of MB onto the ATOB surfaces is easier and more favorable at higher temperatures [60,61].

3.7. Effect of particles size

In adsorption process, particle size and surface area of the adsorbents are the most vital factors affecting the adsorption capacity. The effects of particle size on the removal efficiency of MB were studied focusing on two different size ranges of 210–250 μm and 53–63 μm. As shown in Fig. 7, decreasing the particle size of ATOB adsorbent from the range 210–250 μm to 53–63 μm caused a sharp increase in the removal efficiency of MB dye from 35.1 to 55.2% and from 89.3 to 98.2% using 0.5–5.0 g/L ATOB dosage, respectively. Not surprisingly, the extent of the adsorption process increases as a result of increasing the specific surface areas. The available specific surfaces for adsorption will be greater for smaller particles; hence the adsorption efficiency of MB increases as the particle size decreases. For larger particles, the diffusion resistance to mass transport is higher, and most of the internal particle surfaces may not be utilized for adsorption. Consequently, the amount of adsorbed MB is less. These results demonstrate that smaller particles provide more surface areas and thus increase the adsorption capacity.

3.8. MB adsorption in real wastewater

To investigate the potential removal of MB using ATOB in industries, the adsorption performance was evaluated in a real dye-polluted wastewater. The percentage of dye adsorption by the ATOB surfaces in the synthetic and real wastewaters containing 25, 50, and 100 mg/L concentrations of MB are shown in Fig. 8. Results show that almost no noticeable difference is observed in the adsorption percentage between the synthetic and the real samples at all initial MB concentrations. This means that other substances which are present in the wastewater have no

Table 5
Comparison of adsorption capacity of MB by ATOB other found in the literatures

Adsorbent	q_o (mg/g)	Refs.
Biochar	90.46	This study
Activated carbon	28.5	[42]
Modified pine sawdust	93.5	[43]
Modified loofah	85.5	[44]
Eichhornia crassipes biomass	35.4	[45]
Date palm leaves	58.1	[46]
Raw pine cone	129.9	[47]
Acacia fumosa seed shell	10.5	[48]
Tea waste	85.11	[49]
Fly ash	76.94	[50]
Montmorillonite/$CoFe_2O_4$ composite	76.94	[51]
Orange peel	18.6	[52]
Garlic peel	82.64	[53]
Silica	11.21	[54]
Biochar	12.03	[55]

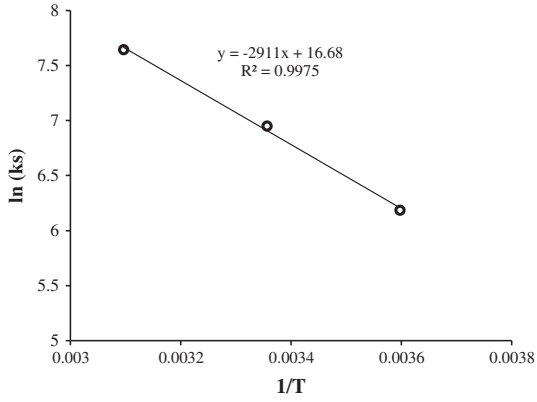

Fig. 6. Plot of ln k_S vs. $1/T$ for the Arrhenius E_a of MB adsorption onto ATOB.

Table 6
The values of thermodynamic parameters of MB adsorption onto ATOB

ΔG° (kJ/mol)				
278	298	323	ΔH° (kJ/mol)	ΔS° (J/mol K)
−22.4	−25.0	−28.0	12.2	124.7

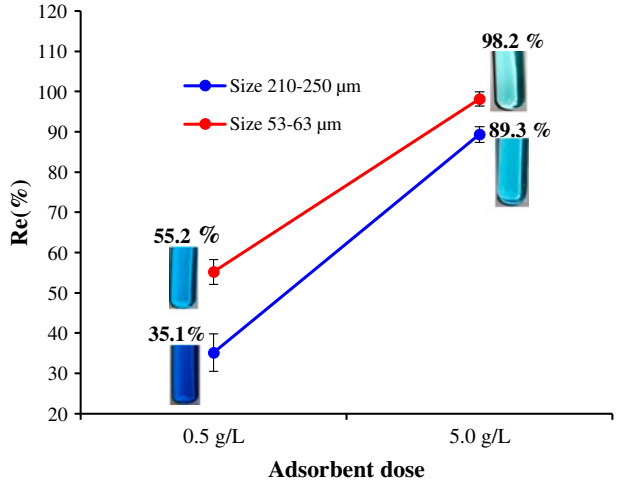

Fig. 7. Effect of particles size of ATOB on MB adsorption percentage (pH 7.0 ± 0.1, contact time: 120 min, MB: 50 mg/L, T = 25 ± 1 ℃).

significant influences on the adsorption percentage of MB onto the ATOB surfaces. These results also suggest that the ATOB enjoys a good potential for the removal of dyes in real samples. Therefore, it can be concluded that the removal of MB dye from industrial wastewaters using the ATOB as a low-cost adsorbent can be both cost-effective and feasible.

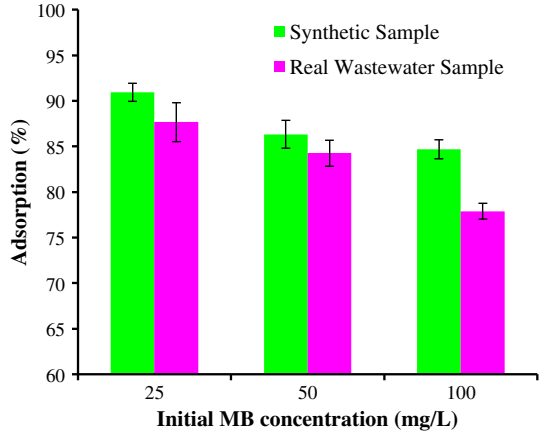

Fig. 8. Comparison of the adsorption MB percentage using ATOB in the synthetic and real wastewaters (pH 7.0 ± 0.1, contact time: 120 min, and adsorbent dose: 10 g/L).

4. Conclusion

In the present study, we used alkaline treated oak wood biochar (ATOB) as a low-cost and locally available material for the preparation of an adsorbent in MB dye adsorption from aqueous solution in a batch system. Results showed that at an optimum pH of 7.0 and an equilibrium reaction time of 60 min, adsorption efficiency witnessed a sharp enhancement by an increase in the temperature and the adsorbent dosage. While, an indirect relationship was observed between MB adsorption efficiency with the initial dye concentration and particles size. The Liu isotherm model provided a better fit than the other applied isotherm models for the adsorption process. The pseudo-second-order model correlated the kinetic data on the ATOB quite well at all initial MB concentrations. The values of the standard Gibbs free energy (ΔG°) and standard enthalpy (ΔH°) obtained from studying the adsorption thermodynamic indicated that MB adsorption onto the ATOB was endothermic and spontaneous. The findings of this research reveal that biochar can be applied as an optimal and efficient adsorbent in the removal of dye from aqueous environments.

Supplementary material

The Supplementary material of this paper is available online at http://dx.doi.10.1080/19443994.2016.1163736.

Acknowledgment

The authors would like to thank the Student Research Committee and the Research and Technology Deputy of Ahvaz Jundishapur University of Medical Sciences for financial support (Grant No. 92.S.10).

References

[1] M. Ghaedi, H. Hossainian, M. Montazerozohori, A. Shokrollahi, F. Shojaipour, M. Soylak, M.K. Purkait, A novel acorn based adsorbent for the removal of brilliant green, Desalination 281 (2011) 226–233.

[2] A. Safavi, S. Momenia, Highly efficient degradation of azo dyes by palladium/hydroxyapatite/Fe_3O_4 nanocatalyst, J. Hazard. Mater. 201–202 (2012) 125–131.

[3] A.A. Babaei, A. Khataee, E. Ahmadpour, M. Sheydaei, B. Kakavandi, Z. Alaee, Optimization of cationic dye adsorption on activated spent tea: Equilibrium, kinetics, thermodynamic and artificial neural network modeling, Korean J. Chem. Eng. 1–10 (in press), doi: 10.1007/s11814-014-0334-6.

[4] M.F. El-Shahat, A.M.A. Shehata, Extraction of p-nitroaniline from aqueous solutions onto activated carbon prepared from treated camphor wood, Int. J. Emerging Technol. Adv. Eng. 4 (2014) 423–4430.

[5] B. Kakavandi, R.R. Kalantary, A.J. Jafari, S. Nasseri, A. Ameri, A. Esrafili, A. Azari, Pb(II) adsorption onto a magnetic composite of activated carbon and superparamagnetic Fe_3O_4 nanoparticles: Experimental and modeling study, CLEAN—Soil Air Water 43 (2015) 1157–1166.

[6] A. Azari, B. Kakavandi, R.R. Kalantary, E. Ahmadi, M. Gholami, Z. Torkshavand, M. Azizi, Rapid and efficient magnetically removal of heavy metals by magnetite-activated carbon composite: A statistical design approach, J. Porous Mater. 22 (2015) 1083–1096.

[7] A.A. Babaei, Z. Baboli, N. Jaafarzadeh, G. Goudarzi, M. Bahrami, M. Ahmadi, Synthesis, performance, and nonlinear modeling of modified nano-sized magnetite for removal of Cr(VI) from aqueous solutions, Desalin. Water Treat. 53 (2015) 768–777.

[8] A.R. Esfahani, A.F. Firouzi, G. Sayyad, A. Kiasat, L. Alidokht, A. Khataee, Pb(II) removal from aqueous solution by polyacrylic acid stabilized zero-valent iron nanoparticles: Process optimization using response surface methodology, Res. Chem. Intermed. 40 (2014) 431–445.

[9] A.R. Esfahani, S. Hojati, A. Azimi, M. Farzadian, A. Khataee, Enhanced hexavalent chromium removal from aqueous solution using a sepiolite-stabilized zero-valent iron nanocomposite: Impact of operational parameters and artificial neural network modeling, J. Taiwan Inst. Chem. Eng. 49 (2015) 172–182.

[10] A.W. Samsuri, F. Sadegh-Zadeh, B.J. Seh-Bardan, Adsorption of As(III) and As(V) by Fe coated biochars and biochars produced from empty fruit bunch and rice husk, J. Environ. Chem. Eng. 1 (2013) 981–988.

[11] A. Örnek, M. Özacar, I.A. Şengil, Adsorption of lead onto formaldehyde or sulphuric acid treated acorn waste: Equilibrium and kinetic studies, Biochem. Eng. J. 37 (2007) 192–200.

[12] W.K. Lafi, Production of activated carbon from acorns and olive seeds, Biomass Bioenergy 20 (2001) 57–62.

[13] J. Jiang, R.-K. Xu, T.-Y. Jiang, Z. Li, Immobilization of Cu(II), Pb(II) and Cd(II) by the addition of rice straw derived biochar to a simulated polluted Ultisol, J. Hazard. Mater. 229–230 (2012) 145–150.

[14] B.H. Hameed, D.K. Mahmoud, A.L. Ahmad, Equilibrium modeling and kinetic studies on the adsorption of basic dye by a low-cost adsorbent: Coconut (Cocos nucifera) bunch waste, J. Hazard. Mater. 158 (2008) 65–72.

[15] E. Agrafioti, D. Kalderis, E. Diamadopoulos, Arsenic and chromium removal from water using biochars derived from rice husk, organic solid wastes and sewage sludge, J. Environ. Manage. 133 (2014) 309–314.

[16] P.J. Mitchell, T.S.L. Dalley, R.J. Helleur, Preliminary laboratory production and characterization of biochars from lignocellulosic municipal waste, J. Anal. Appl. Pyrolysis 99 (2013) 71–78.

[17] J. Pan, J. Jiang, R. Xu, Adsorption of Cr(III) from acidic solutions by crop straw derived biochars, J. Environ. Sci. 25 (2013) 1957–1965.

[18] X. Tong, R. Xu, Removal of Cu(II) from acidic electroplating effluent by biochars generated from crop straws, J. Environ. Sci. 25 (2013) 652–658.

[19] M. Xie, W. Chen, Z. Xu, S. Zheng, D. Zhu, Adsorption of sulfonamides to demineralized pine wood biochars prepared under different thermochemical conditions, Environ. Pollut. 186 (2014) 187–194.

[20] D. Angın, T.E. Köse, U. Selengil, Production and characterization of activated carbon prepared from safflower seed cake biochar and its ability to absorb reactive dyestuff, Appl. Surf. Sci. 280 (2013) 705–710.

[21] Y. Yao, B. Gao, M. Inyang, A.R. Zimmerman, X. Cao, P. Pullammanappallil, L. Yang, Removal of phosphate from aqueous solution by biochar derived from anaerobically digested sugar beet tailings, J. Hazard. Mater. 190 (2011) 501–507.

[22] J. Tang, W. Zhu, R. Kookana, A. Katayama, Characteristics of biochar and its application in remediation of contaminated soil, J. Biosci. Bioeng. 116 (2013) 653–659.

[23] T.-Y. Jiang, J. Jiang, R.-K. Xu, Z. Li, Adsorption of Pb (II) on variable charge soils amended with rice-straw derived biochar, Chemosphere 89 (2012) 249–256.

[24] Y. Wang, L. Wang, G. Fang, H.M.S.K. Herath, Y. Wang, L. Cang, Z. Xie, D. Zhou, Enhanced PCBs sorption on biochars as affected by environmental factors: Humic acid and metal cations, Environ. Pollut. 172 (2013) 86–93.

[25] American Society for Testing and Material (ASTM), Annual book of ASTM, standard test method for performing the sieve analysis of coal and designating coal size, Method D4749.

[26] M.A.P. Cechinel, S.M.A.G. Ulson de Souza, A.A. Ulson de Souza, Study of lead (II) adsorption onto activated carbon originating from cow bone, J. Cleaner Prod. 65 (2013) 342–349.

[27] Y. Yao, F. Xu, M. Chen, Z. Xu, Z. Zhu, Adsorption behavior of methylene blue on carbon nanotubes, Bioresour. Technol. 101 (2010) 3040–3046.

[28] B. Kakavandi, A. Esrafili, A. Mohseni-Bandpi, A.J. Jafari, R.R. Kalantary, Magnetic Fe_3O_4@C nanoparticles as adsorbents for removal of amoxicillin from aqueous solution, Water Sci. Technol. 69 (2014) 147–155.

[29] A. Babaei, Z. Alaee, E. Ahmadpour, A. Ramazanpour-Esfahani, Kinetic modeling of methylene blue adsorption onto acid-activated spent tea: A comparison between linear and non-linear regression analysis, J. Adv. Environ. Health Res. 2 (2014) 197–208.

[30] A. Mohseni-Bandpi, B. Kakavandi, R.R. Kalantary, A. Azari, A. Keramati, Development of a novel magnetite-chitosan composite for the removal of fluoride from drinking water: Adsorption modeling and optimization, RSC Adv. 5 (2015) 73279–73289.
[31] R. Rezaei Kalantry, A. Jonidi Jafari, A. Esrafili, B. Kakavandi, A. Gholizadeh, A. Azari, Optimization and evaluation of reactive dye adsorption on magnetic composite of activated carbon and iron oxide, Desalin. Water Treat. 57 (2016) 6411–6422.
[32] L.D. Prola, E. Acayanka, E.C. Lima, C.S. Umpierres, J.C. Vaghetti, W.O. Santos, S. Laminsi, P.T. Djifon, Comparison of *Jatropha curcas* shells in natural form and treated by non-thermal plasma as biosorbents for removal of Reactive Red 120 textile dye from aqueous solution, Ind. Crops Prod. 46 (2013) 328–340.
[33] M.C. Ribas, M.A. Adebayo, L.D. Prola, E.C. Lima, R. Cataluña, L.A. Feris, M. Puchana-Rosero, F.M. Machado, F.A. Pavan, T. Calvete, Comparison of a homemade cocoa shell activated carbon with commercial activated carbon for the removal of reactive violet 5 dye from aqueous solutions, Chem. Eng. J. 248 (2014) 315–326.
[34] M.K. Hossain, V. Strezov, K.Y. Chan, A. Ziolkowski, P.F. Nelson, Influence of pyrolysis temperature on production and nutrient properties of wastewater sludge biochar, J. Environ. Manage. 92 (2011) 223–228.
[35] D. Mohan, C.U. Pittman Jr, M. Bricka, F. Smith, B. Yancey, J. Mohammad, P.H. Steele, M.F. Alexandre-Franco, V. Gómez-Serrano, H. Gong, Sorption of arsenic, cadmium, and lead by chars produced from fast pyrolysis of wood and bark during bio-oil production, J. Colloid Interface Sci. 310 (2007) 57–73.
[36] D. Mohan, H. Kumar, A. Sarswat, M. Alexandre-Franco, C.U. Pittman Jr, Cadmium and lead remediation using magnetic oak wood and oak bark fast pyrolysis biochars, Chem. Eng. J. 236 (2014) 513–528.
[37] A. Ramazanpour Esfahani, A. Farrokhian Firouzi, Synthesis and application of stabilized zero-valent iron nanoparticles for hexavalent chromium removal in saturated sand columns: Experimental and modeling studies, Desalin. Water Treat. (in press), doi: 10.1080/19443994.2015.1072842.
[38] A.R. Esfahani, A.F. Firouzi, G. Sayyad, A. Kiasat, Transport and retention of polymer-stabilized zero-valent iron nanoparticles in saturated porous media: Effects of initial particle concentration and ionic strength, J. Ind. Eng. Chem. 20 (2014) 2671–2679.
[39] M. Zhao, P. Liu, Adsorption of methylene blue from aqueous solutions by modified expanded graphite powder, Desalination 249 (2009) 331–336.
[40] D. Kavitha, C. Namasivayam, Experimental and kinetic studies on methylene blue adsorption by coir pith carbon, Bioresour. Technol. 98 (2007) 14–21.
[41] E. Malkoc, Y. Nuhoglu, Investigations of nickel(II) removal from aqueous solutions using tea factory waste, J. Hazard. Mater. 127 (2005) 120–128.
[42] P.M.K. Reddy, K. Krushnamurty, S. Mahammadunnisa, A. Dayamani, C. Subrahmanyam, Preparation of activated carbons from bio-waste: Effect of surface functional groups on methylene blue adsorption, Int. J. Environ. Sci. Technol. 12 (2015) 1363–1372.
[43] R. Zhang, Y. Zhou, X. Gu, J. Lu, Competitive adsorption of methylene blue and Cu^{2+} onto citric acid modified pine sawdust, CLEAN–Soil Air Water 43 (2015) 96–103.
[44] J.-X. Yu, L.-Y. Wang, R.-A. Chi, Y.-F. Zhang, Z.-G. Xu, J. Guo, Removal of cationic dyes: Basic magenta and methylene blue from aqueous solution by adsorption on modified loofah, Res. Chem. Intermed. 39 (2013) 3775–3790.
[45] W.C. Wanyonyi, J.M. Onyari, P.M. Shiundu, Adsorption of methylene blue dye from aqueous solutions using eichhornia crassipes, Bull. Environ. Contam. Toxicol. 91 (2013) 362–366.
[46] M. Gouamid, M. Ouahrani, M. Bensaci, Adsorption equilibrium, kinetics and thermodynamics of methylene blue from aqueous solutions using date palm leaves, Energy Procedia 36 (2013) 898–907.
[47] M.T. Yagub, T.K. Sen, M. Ang, Removal of cationic dye methylene blue (MB) from aqueous solution by ground raw and base modified pine cone powder, Environ. Earth Sci. 71 (2014) 1507–1519.
[48] M. Kumar, R. Tamilarasan, Modeling studies for the removal of methylene blue from aqueous solution using *Acacia fumosa* seed shell activated carbon, J. Environ. Chem. Eng. 1 (2013) 1108–1116.
[49] C. Woolard, J. Strong, C. Erasmus, Evaluation of the use of modified coal ash as a potential sorbent for organic waste streams, Appl. Geochem. 17 (2002) 1159–1164.
[50] M. Al-Ghouti, M. Khraisheh, S. Allen, M. Ahmad, The removal of dyes from textile wastewater: A study of the physical characteristics and adsorption mechanisms of diatomaceous earth, J. Environ. Manage. 69 (2003) 229–238.
[51] L. Ai, Y. Zhou, J. Jiang, Removal of methylene blue from aqueous solution by montmorillonite/$CoFe_2O_4$ composite with magnetic separation performance, Desalination 266 (2011) 72–77.
[52] C. Namasivayam, S. Sumithra, Removal of direct red 12B and methylene blue from water by adsorption onto Fe (III)/Cr (III) hydroxide, an industrial solid waste, J. Environ. Manage. 74 (2005) 207–215.
[53] M.T. Uddin, M.A. Islam, S. Mahmud, M. Rukanuzzaman, Adsorptive removal of methylene blue by tea waste, J. Hazard. Mater. 164 (2009) 53–60.
[54] P. Janos, H. Buchtová, M. Rýznarová, Sorption of dyes from aqueous solutions onto fly ash, Water Res. 37 (2003) 4938–4944.
[55] Y. Liu, X. Zhao, J. Li, D. Ma, R. Han, Characterization of bio-char from pyrolysis of wheat straw and its evaluation on methylene blue adsorption, Desalin. Water Treat. 46 (2012) 115–123.
[56] Y. Seki, K. Yurdakoç, Adsorption of promethazine hydrochloride with KSF montmorillonite, Adsorption 12 (2006) 89–100.
[57] M. Kara, H. Yuzer, E. Sabah, M. Celik, Adsorption of cobalt from aqueous solutions onto sepiolite, Water Res. 37 (2003) 224–232.
[58] B. Kakavandi, A. Jonidi Jafari, R. Rezaei Kalantary, S. Nasseri, A. Esrafili, A. Gholizadeh, A. Azari, Simultaneous adsorption of lead and aniline onto magnetically recoverable carbon: Optimization, modeling and

mechanism, J. Chem. Technol. Biotechnol. (in press), doi: 10.1002/jctb.4925.
[59] M.Ş. Tanyildizi, Modeling of adsorption isotherms and kinetics of reactive dye from aqueous solution by peanut hull, Chem. Eng. J. 168 (2011) 1234–1240.
[60] M. Massoudinejad, A. Asadi, M. Vosoughi, M. Gholami, B. Kakavandi, M. Karami, A comprehensive study (kinetic, thermodynamic and equilibrium) of arsenic (V) adsorption using KMnO4 modified clinoptilolite, Korean J. Chem. Eng. 32 (2015) 2078–2086.
[61] B. Kakavandi, R. Rezaei Kalantary, M. Farzadkia, A.H. Mahvi, A. Esrafili, A. Azari, A.R. Yari, A.B. Javid, Enhanced chromium (VI) removal using activated carbon modified by zero valent iron and silver bimetallic nanoparticles, J. Environ. Health Sci. Eng. 12 (2014) 1–10.